Proceedings of the 17th World Congress
The International Federation of Automatic Control
Seoul, Korea, July 6-11, 2008

Adaptive Feed-Forward Cancellation Control of a Full-Bridge DC-AC Voltage Inverter ⋆

Shane Malo and Robert Griñó

Institut d'Organització i Control de Sistemes Industrials (IOC), Universitat Politècnica de Catalunya (UPC), Barcelona, Spain.
e-mail: {shane.malo,roberto.grino}@upc.edu

Abstract: Dc-ac inverters are needed in many applications. The full-bridge dc-ac inverter has been widely used in industry applications and trough the literature. If the nature of the load is not known *a priori*, some considerations should be taken in order to assure the quality of service to be provided by the inverter. When nonlinear loads are fed by a full-bridge dc-ac inverter, odd harmonics of the fundamental ac frequency are introduced into the output voltage shape. For the purpose of producing a good sinusoidal output voltage signal, the control strategy must be able to reject periodic output disturbances. Adaptive Feed-forward Cancellation (AFC) is a control technique that has been successfully used to selectively reject periodic output disturbances in continuous-time mechanical systems. This paper deals with the use of AFC to control the output voltage of an electrical system, in this case, a dc-ac full-bridge inverter, to produce a standard European ac voltage signal, 230 Vrms and 50 Hz, accomplishing the design of the controller directly in the z-domain.

1. INTRODUCTION

Feeding an isolated load with a dc-ac inversion system is a challenging task, generally due to the lack of knowledge about the nature of the load (linear or nonlinear), and the necessity of keeping the desired output voltage characteristics (frequency, amplitude, THD, etc.) within certain limits that determine the quality of service to be provided. Non-linear loads, such as diode rectifiers and fluorescent lights with electronic ballasts, introduce odd harmonics of the fundamental ac frequency (Pileggi et al. (1993)), generally 50 Hz or 60 Hz, into the output voltage shape of the dc-ac inversion system. Adaptive Feed-forward Cancellation (AFC) is a control technique that allows the designer to reject or attenuate, in a selective manner, specific harmonics of periodic disturbance signals. AFC has successfully been used in mechanical systems (Ludwick (1999); Bodson (2005); Byl et al. (2005)), to reject periodic disturbances that are harmonics of some fundamental frequency. It is interesting to note that under certain circumstances (Bodson et al. (1992, 1994)), the AFC problem becomes equivalent to that of the Internal Model Principle (IMP) (Francis and Mohan (1976)), and therefore, perfect disturbance rejection of the selected harmonics can be expected. The IMP states that a model of the disturbance must be included into the open-loop transfer function, requiring then, previous knowledge of the disturbance signal. The design and the equivalence of controllers between the AFC and IMP schemes were treated by Messner and Bodson (1994) and Bodson (2004), and a loop shaping approach is given by Byl et al. (2005) in order to help the designer in the selection of the design parameters.

2. DISCRETE-TIME AFC

The AFC approaches treated by Bodson et al. (1992, 1994); Messner and Bodson (1994); Ludwick (1999); Bodson (2004, 2005); Byl et al. (2005) assume continuous-time variables and controller design, although in practice, almost all controllers need to be implemented by means of digital computers, and hence, in discrete time. This work deals with the design of an AFC controller directly in the z-domain.

In the continuous-time framework, the advantage on the use of the AFC control structure to reject periodic disturbances lies in the placement of an infinite gain on the open-loop transfer function at the desired ω_k frequency by means of the $R_k(s)$ resonator. By following the IMP, perfect disturbance rejection at such frequency can be expected. In order to obtain a feasible discrete-time realization, it needs to be shown that the main characteristics of the continuous-time realization are preserved. Fig.1 shows the block diagram of the AFC closed loop. A proportional block with constant K_0 is added in order to help the reference tracking. Fig.2 shows block diagram for the proposed discrete-time resonator.

2.1 Construction of the Discrete-Time Resonator $R_k(z)$: The main difference between the continuous-time and the discrete-time realizations of the AFC controller resides in the construction of the $R_k(z)$ resonator modules. The $H(z)$ block in Fig.2 can be any discrete-time integrator structure. The resonator shown in Fig.2 can be expressed by the z-domain transfer function (1).

$$R_k(z) = \frac{1}{2} g_k \left[H(z e^{-j\omega_k T}) e^{-j\varphi_k} + H(z e^{j\omega_k T}) e^{j\varphi_k} \right] \quad (1)$$

⋆ This work has been partially supported by the Spanish "Ministerio de Educación y Ciencia (MEC)" under project DPI2004-06871-C02-02. The work of the first author is supported by the "Departament d'Universitats, Recerca i Societat de la Informació" of the "Generalitat de Catalunya" and the European Social Fund by means of a FI scholarhip (Beca Predoctoral per a la Formació de Personal Investigador) with expedient number 2007FIR 00118.

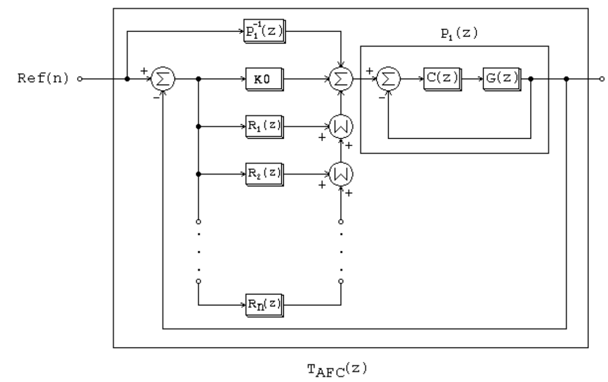

Fig. 1. Discrete-time AFC closed loop.

In this work, a Backward Euler integrator has been chosen for the $H(z)$ block, as seen in (2).

$$H(z) = \frac{z}{(z-1)} \tag{2}$$

By replacing (2) into (1) and simplifying, the z-domain transfer function of the resonator becomes

$$R_k(z) = g_k \frac{\cos(\varphi_k)z^2 - \cos(\omega_k T + \varphi_k)z}{z^2 - 2\cos(\omega_k T)z + 1} \tag{3}$$

Equation (3) shows the resulting structure for the discrete-time resonator implementation by selecting the first order structure (2) as integrator. The parameters involved in the discrete-time resonator structure are: g_k, ω_k, φ_k and T. Where g_k is a positive real gain, ω_k is the frequency, in rad/s at which the desired resonating gain is to be placed, φ_k is the phase shift parameter for kth resonator in rads, and finally T is the sampling period in seconds for the discrete-time system.

2.2 Phase of the resonator $R_k(z)$ at the resonating frequency ω_k:

First, the phase and gain characteristics of the discrete time resonator at the ω_k frequency are explored. The behavior of the system around the resonating frequency ω_k can be studied departing from (1).

When the continuous-time frequency ω approaches ω_k, the discrete time variable z becomes $z = e^{j(\omega_k T + \varepsilon)}$, for a sufficiently small value of $|\varepsilon| \geq 0$. Having substituted this value in (1) and simplifying, the resonator structure becomes:

$$R_k(z) = \frac{1}{2} g_k \left[H(e^{j\varepsilon})e^{-j\varphi_k} + H(e^{j(2\omega_k T + \varepsilon)})e^{j\varphi_k} \right] \tag{4}$$

By substituting (2) in (4) the first half of (4) can be rewritten as:

$$\frac{1}{2} g_k \left[H(e^{j\varepsilon})e^{-j\varphi_k} \right] = \frac{1}{4} g_k \left[\frac{e^{j(\frac{\varepsilon}{2} - \frac{\pi}{2} - \varphi_k)}}{sin(\frac{\varepsilon}{2})} \right] \tag{5}$$

For the sake of simplicity, let us assume a unitary gain $g_k = 1$. As ε approaches zero from either right or left sides, the modulus of (5) goes to infinite, as the denominator $sin(\varepsilon/2)$ goes to zero. The effects of the second half of (4) are marginal at this point, and (5) dominates the behavior of the resonator structure $R_k(z)$.

When ε approaches zero from the left, which is equivalent to say that the input frequency approaches the resonating

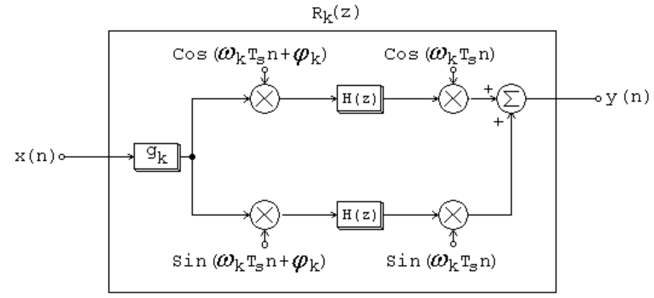

Fig. 2. Discrete-time AFC resonator structure.

frequency from the left ($\omega \to \omega_k^-$), the phase shift of the system becomes

$$\angle\ R_k(e^{j\omega T})\big|_{\omega \to \omega_k^-} = -\varphi_k + \frac{\pi}{2}$$

When ε approaches zero from the right, the phase component of the resonator structure becomes

$$\angle\ R_k(e^{j\omega T})\big|_{\omega \to \omega_k^+} = -\varphi_k - \frac{\pi}{2}$$

Therefore, the phase shift of the resonator at the resonating frequency ω_k, is the average of the phase shifts of the resonator when ω approaches ω_k from the right and from the left, hence

$$\angle R_k(e^{j\omega_k T}) = -\varphi_k \tag{6}$$

2.3 Phase of the resonator $R_k(z)$ at $\omega = 0$ and $\omega = \pi/T$:

Let us now inspect the phase characteristics of the resonator structure at the dc frequency. When $\omega = 0$, then $z = e^{j\ 0T} = 1$ and (3) takes the form:

$$R_k(1) = g_k \frac{\cos(\varphi_k) - \cos(\omega_k T + \varphi_k)}{2 - 2\cos(\omega_k T)} \tag{7}$$

Let us assume $g_k = 1$. All the values in the equation above are real, and therefore $R_k(1)$ is a real number. A deeper inspection on the values would be necessary to determine the phase of such quantity.

The resonating frequency ω_k lies within the operating band and therefore $0 < \omega_k < \pi/T$, and then the denominator $(2 - 2\cos(\omega_k T))$ is always greater than zero, as the $\cos(\omega_k T)$ value is always lower than 1. In the numerator $(\cos(\varphi_k) - \cos(\omega_k T + \varphi_k))$, the ω_k frequency is fixed as the independent variable, as this value is determined by the disturbance frequency to be rejected. The sampling period T is fixed as well. The sign change conditions can be examined by looking at the locations of the zero crossings of the numerator. From the assumptions above the following phase conditions are imposed over $R_k(1)$.

$$\angle R_k(1) = \begin{cases} \pi\ if\ \varphi_k < -\omega_k T/2 \\ 0\ if\ \varphi_k > -\omega_k T/2 \end{cases} \tag{8}$$

At the maximum allowed frequency by the discrete-time system a similar analysis can be performed. When $\omega = \pi/T$, $z = -1$, (3) takes the form:

$$R_k(-1) = g_k \frac{\cos(\varphi_k) + \cos(\omega_k T + \varphi_k)}{2 + 2\cos(\omega_k T)} \tag{9}$$

In this case the denominator $(2+2\cos(\omega_k T))$ is always positive. When examining the numerator $(\cos(\varphi_k)+\cos(\omega_k T+$

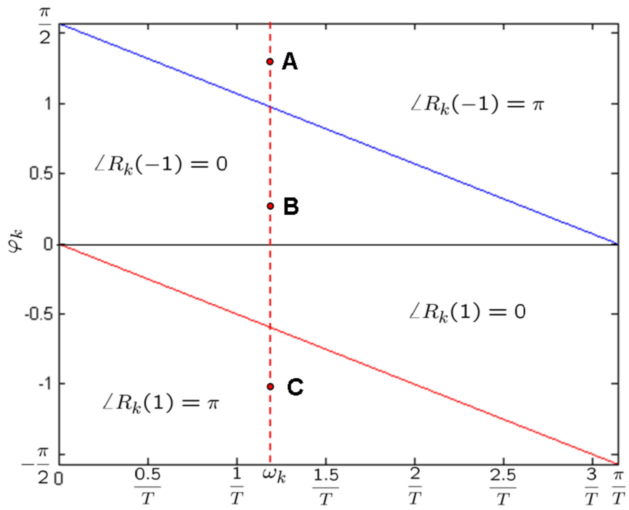

Fig. 3. Phase shift boundaries for $\omega = 0$ and $\omega = \pi/T$ for the discrete time resonator structure $R_k(z)$

φ_k)), the following conditions are derived from fixing ω_k as independent variable, with T fixed by the hardware constraints:

$$\angle R_k(-1) = \begin{cases} 0 \ if \ \varphi_k < (\pi - \omega_k T)/2 \\ \pi \ if \ \varphi_k > (\pi - \omega_k T)/2 \end{cases} \quad (10)$$

From the conditions above, it can be concluded that the resonator structure will have a phase drop of $-\pi$ rad at the resonating frequency ω_k, and the shift will be centered at $-\varphi_k$ as stated in (6). The phase value at the beginning ($\omega = 0$) and at the end of the band ($\omega = \pi/T$) will be determined by (8) and (10).

A single resonator $R_k(z)$ can show three different combinations for the phase value at the start ($\angle R_k(1)$) and at the end of the band ($\angle R_k(-1)$) depending on the selection of ω_k and φ_k. Fig. 3 shows the phase shift boundaries for the discrete time resonator structure $R_k(z)$ as a function of the resonating frequency ω_k. The upper line shows the boundary condition imposed to $\angle R_k(-1)$ ($\omega = \pi/T$) by (10). The lower line shows the boundary condition imposed to $\angle R_k(1)$ ($\omega = 0$) by (8). As can be seen, a single resonator can change its start and finish phase values depending on the selection of the φ_k parameter. If $\varphi_k = \text{A}$ is chosen (see Fig. 3), the start and finish phase values will be $\angle R_k(1) = 0$ and $\angle R_k(-1) = \pi$ respectively. If $\varphi_k = \text{B}$ the start and finish angles would be, $\angle R_k(1) = 0$ and $\angle R_k(-1) = 0$. If $\varphi_k = \text{C}$, then $\angle R_k(1) = \pi$ and $\angle R_k(-1) = 0$.

Fig. 4 shows the effect on the change of the phase shift parameter φ_k above or below the boundaries of Fig. 3. In this case a resonating frequency of $\omega_k = 10,000$ rad/s has been chosen, the sampling frequency is 20,000 Hz which produces a sampling period of $T = 50\ \mu$s, a unitary gain g_k has been used, and three different values for the parameter φ_k have been considered. The φ_k values considered were, $\varphi_k = 1.396$ rad lying in the A region of Fig. 3, producing the red trace in Fig. 4. The $\varphi_k = 0$ rad value lies in the B region, and produces the green trace, and $\varphi_k = -0.349$ rad lies in the C region producing the blue trace. It is interesting to note that for the lower frequency range, when the resonating frequency ω_k is farther from the end of the band value ($\omega = \pi/T$), the phase shift conditions

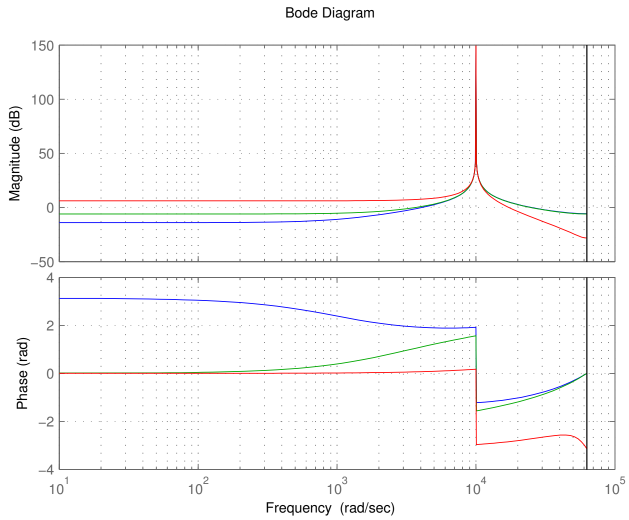

Fig. 4. Bode diagram for a single resonator $R_k(z)$ using different values for the phase shift parameter φ_k(-0.349 rad, 0 rad and 1.396 rad), $g_k = 1$, $\omega_k = 10,000$ rad/s , $T = 50\ \mu$s.

are equivalent to the continuous-time conditions given by Byl et al. (2005). Conversely, these conditions will be equivalent if the sampling period trends to zero, which will make the discrete-time system response trend to the continuous-time one.

2.4 Gain characteristics of $R_k(z)$ at $\omega = 0$ and $\omega = \pi/T$:

From (7) the gain characteristics at $\omega = 0$ can be analyzed. Again, the values of ω_k and T are fixed by the conditions imposed by the problem to be solved. The phase shift parameter φ_k is the independent variable. The gain growth or decrease regions at $\omega = 0$ ($|R_k(1)|$) can be determined by examining the location of the sign changes (see Fig. 3) and the inflection points of (7) respect to the parameter φ_k. Assuming $g_k = 1$, only one inflection point is found for $R_k(1)$ ($\omega = 0$) when varying φ_k. This point is located at $(\pi - \omega_k T)/2$ having positive slope before the inflection point and negative slope after it.

It is also necessary to take into account the phase change conditions expressed in Fig. 3 for $R_k(1)$. These conditions have an straight forward interpretation respect to its relationship with the sign of $R_k(1)$. If $\angle R_k(1) = \pi$, then $R_k(1) < 0$ and if $\angle R_k(1) = 0$, therefore $R_k(1) > 0$. If a decrease in the value of φ_k produces an increase on $|R_k(1)|$ this increase will happen until φ_k reaches the inflection point at $(\pi - \omega_k T)/2$, and after the inflection point, a decrease on $|R_k(1)|$ must happen, until the sign change condition ($\angle R_k(1)$ changes from 0 to π) is reached at $-\omega_k T/2$. At $\varphi_k = -\omega_k T/2 \Rightarrow R_k(1) = 0$, and if φ_k continues decreasing, then $|R_k(1)|$ must increase again.

The relationship between the growth/decrease on the gain of the resonator $R_k(z)$ in function of ω_k at $\omega = 0$ can be summarized as follows:

- $|R_k(1)|$ decreases if φ_k increases and $\varphi_k > -\omega_k T/2$.
- $|R_k(1)|$ increases if φ_k increases and $-\omega_k T/2 < \varphi_k < (\pi - \omega_k T)/2$.
- $|R_k(1)|$ decreases if φ_k increases and $\varphi_k > (\pi - \omega_k T)/2$.

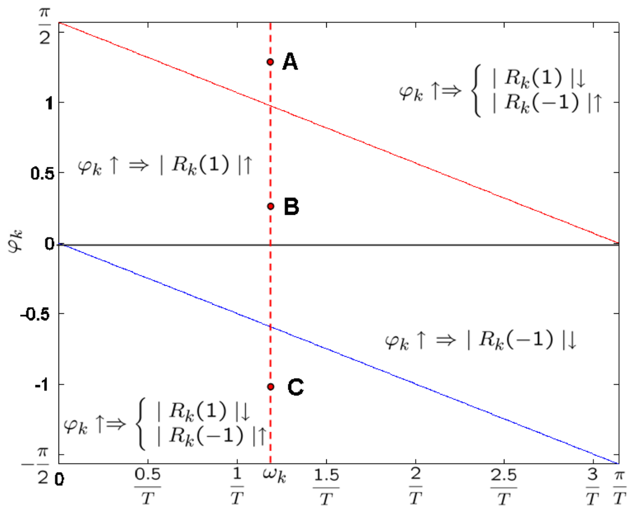

Fig. 5. Gain growth/decrease boundaries for $\omega = 0$ and $\omega = \pi/T$ for the discrete time resonator structure $R_k(z)$

A similar analysis can be performed for the frequency at the end of the allowed band, where $\omega = \pi/T$, $z = -1$. In this case the gain increase/decrease characteristics can be studied departing from (9). Again, ω_k and T are fixed by the problem statement and $g_k = 1$. The gain increase/decrease characteristics can be examined by determining the location of the sign changes (see Fig. 3) and the inflection points and of (9) respect to φ_k. Only one inflection point is found at $-\omega_k T/2$, when varying φ_k, and the sign change condition is located at $(\pi - \omega_k T)/2$. In this case the increase/decrease relationship can be summarized as follows

- $|R_k(-1)|$ increases if φ_k increases and $\varphi_k < -\omega_k T/2$
- $|R_k(-1)|$ decreases if φ_k increases and $-\omega_k T/2 < \varphi_k < (\pi - \omega_k T)/2$
- $|R_k(-1)|$ increases if φ_k increases and $\varphi_k > (\pi - \omega_k T)/2$

The relationships imposed over the growth/decrease of $|R_z(1)|$ $(\omega = 0)$ and $|R_z(-1)|$ $(\omega = \pi/T)$ are summarized in Fig. 5. The upper line shows the location of the inflection point of $R_z(1)$ when varying φ_k as a function of ω_k. The lower line shows the location of the inflection point of $R_z(-1)$ when varying φ_k as a function of ω_k. It is interesting to note that the location of the inflection points of $R_k(1)$ and $R_k(-1)$ as a function of ω_k coincides with the location of the phase change boundaries presented in Fig. 3. For a single resonator $R_k(z)$ with resonating frequency ω_k, if φ_k is chosen to lie in the A area, an increase on the value of φ_k will cause a decrease in $|R_z(1)|$ and an increase on the value of $|R_z(-1)|$. If φ_k is chosen to lie in the B area, an increase on its value will cause an increase in $|R_z(1)|$ and a decrease $|R_z(-1)|$. If φ_k is chosen to lie in the C area, an increase on its value will cause a decrease in $|R_z(1)|$ and an increase in $|R_z(-1)|$.

Fig. 6 shows the effect over the gain and phase characteristics for a single resonator $R_k(z)$ with resonating frequency $\omega_k = 100$ rad/s, sampling period $T = 50$ μs, unitary g_k gain and changes applied to the φ_k value within the B region. As can be appreciated, with values of φ_k lying within the B region, the start $(\angle R_k(1))$ and finish

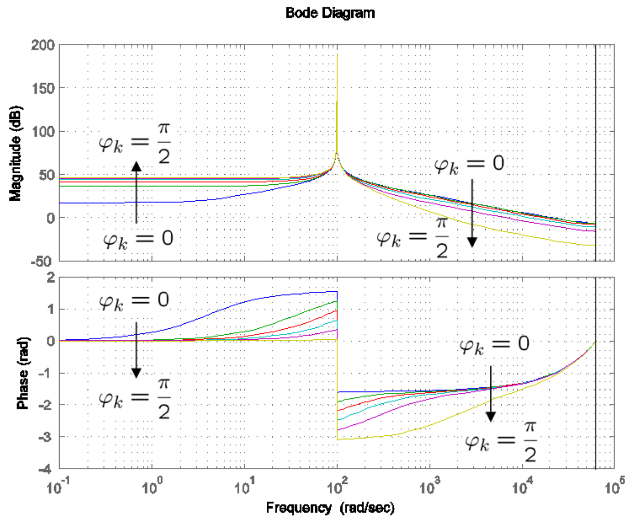

Fig. 6. Effect of the change on the phase shift parameter φ_k within the B region on a single $R_k(z)$ resonator, with $\omega_k = 100$ rad/s, $T = 50$ μs and $g_k = 1$ ($\varphi_k = 0.0349$ rad, 0.3316 rad, 0.6283 rad, 0.9250 rad, 1.2217 rad and 1.5184 rad).

$(\angle R_k(-1))$ phases of the resonator are located at 0 rad. The upper boundary for $|R_k(1)|$ is located at $1.5683 \approx \pi/2$ rad, and the lower boundary for $|R_k(-1)|$ is located at $-0.0025 \approx 0$ rad. The angles used to change the φ_k values are: 0.0349 rad, 0.3316 rad, 0.6283 rad, 0.9250 rad, 1.2217 rad and 1.5184 rad. It can be noted in that as φ_k increases, $|R_k(1)|$ increases, and $|R_k(-1)|$ decreases as stated in Fig. 5.

3. THE DC-AC INVERTER PROBLEM

Isolated electric energy generation systems are often needed to supply electric loads where the electrical network is not available or suitable for the application. This could be caused due to geographic isolation, the necessity of load mobility, demanded values of voltage and current that are not compatible with the local networks, etc.. This makes the design and construction of stand-alone energy generation systems a must. It is very usual that the loads to be fed require ac voltages, and therefore, special attention must be taken when designing ac output stages. Often, stand alone energy generation systems generate the ac output signal departing from a dc power source, such as batteries, photovoltaic arrays or fuel cells. This work deals with the analysis, design and control of a dc-ac inversion stage, which will be in charge of providing a high quality ac output signal departing from a dc source. The loads to be fed are isolated, and therefore, the system itself must be capable of maintaining the quality of service indicators within acceptable levels.

A standard full-bridge dc-ac inverter topology has been chosen. This topology has been widely used through the literature and in industrial applications due to its high reliability and relatively simple structure.

3.1 Description of the plant:

Fig. (7) shows the plant to be controlled by the discrete-time AFC control scheme. The experimental prototype works using three-level single-update centered pulse PWM

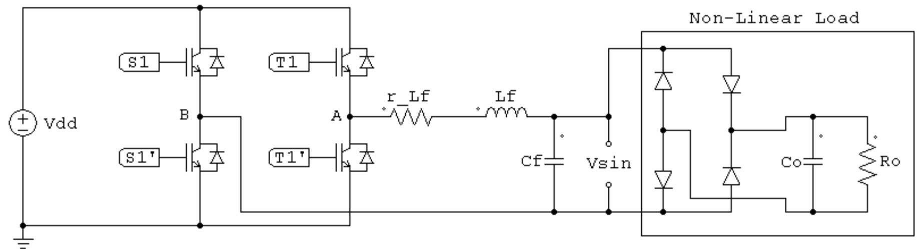

Fig. 7. Full-bridge DC-AC inverter with a non-linear load (full-bridge diode rectifier with a RC load).

(Pulse Width Modulation). This PWM technique offer some advantages such as reduction of the harmonic content of the switching frequency (Holmes and Lipo (2003)) and only one duty cycle command is generated to control the two legs that form the full-bridge inverter. Under this assumptions the averaged behavior of the system can be expressed in the following form:

$$\begin{bmatrix} \dot{v}_{C_f} \\ \dot{i}_{L_f} \end{bmatrix} = \begin{bmatrix} 0 & 1/C_f \\ -1/L_f & -r_{L_f}/L_f \end{bmatrix} \begin{bmatrix} v_{C_f} \\ i_{L_f} \end{bmatrix} + \begin{bmatrix} 0 \\ V_{dd}/L_f \end{bmatrix} u$$

$$v_o = [\,1\ 0\,] \begin{bmatrix} v_{C_f} \\ i_{L_f} \end{bmatrix}$$

$$\text{with } u \in [-1, 1] \qquad (11)$$

From (11) the following transfer function that models the behavior of the system from the averaged duty cycle u to the output voltage is obtained

$$G(s) = \frac{V_o}{U} = \frac{V_{dd}}{C_f\ L_f\ s^2 + C_f\ r_{L_f}\ s + 1} \qquad (12)$$

4. CONTROLLER DESIGN

This new approach on the AFC controller design has been used to control the output voltage of a full-bridge dc-ac inverter (see Fig.7), following the loop-shaping approach presented in Byl et al. (2005). The output voltage must follow a sinusoidal reference with a fundamental frequency of 50 Hz and 230 Vrms. Disturbance rejection has been planned to take place in the first 30 harmonics and the inner closed loop has been designed to provide as much bandwidth as possible.

The plant to be controlled is in this case the discrete-time transfer function[1] $G(z) = \mathfrak{Z}\{ZOH(s)G(s)\}$. Where $ZOH(s)$ is a zero-order hold used as holding device with a sampling period of $T = 50$ μs. A controller ($C(z) = 0.0098(z^2 - 1.837z + 0.9129)/((z - 0.856)(z - 0.078))$) has been designed for the inner loop. The stability margins for the inner open-loop transfer function $L(z) = C(z)G(z)$ show acceptable levels, having a gain margin of 19.3 dB and a phase margin of 47^o. The norm $||S_1(z)||_\infty$ lies below 5 dB with $S_1(z) = 1/(1 + C(z)G(z))$, which represents a good robustness indicator for the inner loop (Doyle et al. (1990)). The inner closed-loop transfer function $P_1(z) = C(z)G(z)/(1 + C(z)G(z))$ acts as the new plant to be controlled by the discrete-time AFC approach. As stated in section 2.2, the phase shift of the resonator $R_k(z)$ at the ω_k frequency will be centered at $-\varphi_k$. As in the continuous time case presented by Byl et al. (2005), a selection of $\varphi_k = \angle P_1(z_k)$ with $z_k = e^{j\omega_k T}$ will cause the AFC transmission loop to center all the phase shifts around 0^o, and therefore providing the system of the highest phase margin available.

The parameters g_k have been chosen by using a hyperbolic profile, giving more gain to the low frequencies and less gain to the high frequencies. This shape allows the control system to provide the highest energy levels to the region of the fundamental frequency and the lower harmonics where the highest levels of disturbance are usually located.

The feed-forward path $P_1^{-1}(z)$ will reinforce the tracking of the reference signal. As in this case the reference signal is a fixed 50 Hz (fundamental frequency) sinusoid, a constant value of $P_1^{-1}(z) = 1/(P_1(z_1))$ with $z_1 = e^{j\omega_1 T}|_{\omega_1 = 2\pi 50}$ has been chosen, and finally the proportional path K_0 has a value of 0.01. The closed-loop system shows gain and phase margins within good levels while keeping good rejection at the desired harmonics. An overall gain margin of 17.80 dB, and a phase margin of 82.58^o are obtained and $||S_{AFC}(z)||_\infty$ lies below 5 dB with $S_{AFC}(z) = 1/(1 + C_{AFC}(z)P_1(z))$.

Fig. 8 shows the Bode plot for the AFC transmission loop $L_{AFC}(z) = C_{AFC}(z)P_1(z)$ where

$$C_{AFC}(z) = K_0 + \sum_{k=1}^{30} R_k(z)$$

As can be seen from Fig. 8 there are 30 resonant peaks at 50 Hz and its respective harmonics. The phase shifts are all centered at 0^o, which guarantees the maximum phase margin on the system.

5. EXPERIMENTAL RESULTS

Fig. 9 shows the output voltage and current waveforms for the switched dc-ac voltage inverter system when feeding a full-bridge diode rectifier with a C filter and a R load at full load (4.07 kVA). Fig. 10 shows that the total harmonic distortion (THD[2]) of the output voltage does not exceed 0.2% while the output (rectifier) current has a rms value of 26.43 A and a peak value of 73.5A, having then a CF of 2.78 and a THD of 73.5%. Load change tests have been performed from 0 kVA up to 1 kVA output power and viceversa, in both cases the settling time for the amplitude of the output voltage is less than 140 ms. The experimentation was performed over the prototype, at 20 kHz, using pulse width modulation (PWM) with centered pulse. A 2 μs dead time was included at the PWM module complementary signals. The components used in

[1] The quantities used are the following: $V_{dd} = 425$ V, $L_f = 384.00$ μH, r_{L_f}=700 mΩ, $C_f = 81.00$ μF, $C_o = 6400$ μF, $R_o = 24$ Ω. These quantities correspond to the values of the components installed in the experimental setup.

[2] The THD is calculated with respect to the rms value of the of signal being measured, therefore, the THD ranges from 0% to 100%.

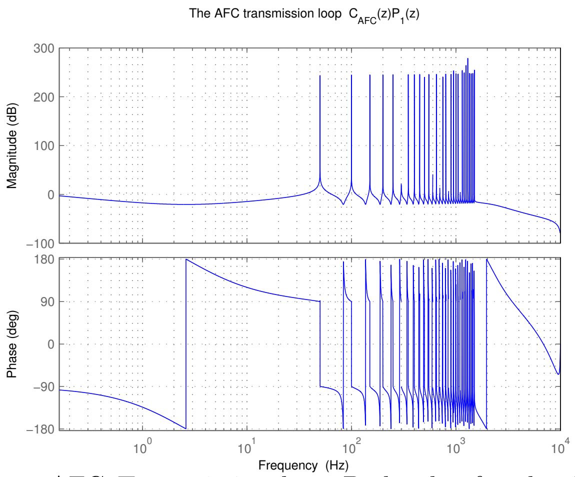

Fig. 8. AFC Transmission loop Bode plot for the dc-ac inversion system.

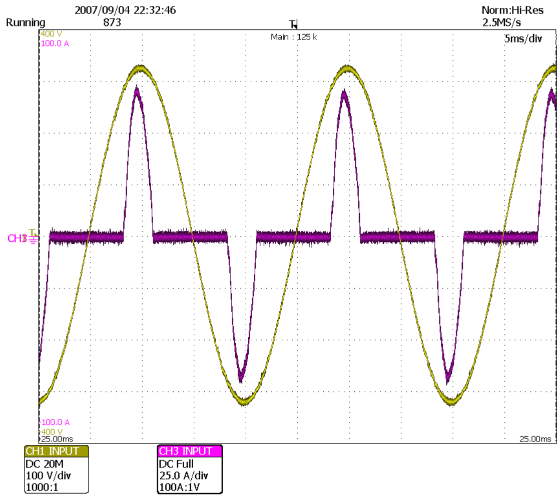

Fig. 9. Output voltage and current shapes for the inverter feeding the nonlinear load (diode rectifier with R load and Co filter) at 4.0 kVA.

the nonlinear load used in the test have been dimensioned following the guidelines provided by the IEC (1999) for the test of UPS (Uninterruptible Power Systems).

6. CONCLUSIONS

The rejection of each harmonic can be improved by selectively increasing the gain g_k in the appropriate resonator $R_k(z)$. As the phase advance parameters have been selected according to the phase value in the inner closed loop ($P_1(z)$), the only design parameters that remain free to adjust are the gains g_k of the resonators and the proportional parameter K_0. It is important to note that the differences between the behavior of the resonator in the continuous-time case and the discrete-time case will be higher as the resonant frequency ω_k approaches the end of the frequency band π/T. Although the diode rectifier demands large amounts of current from the inverter at the odd harmonics of the fundamental ac frequency, the low output voltage THD achieved at full-load condition confirms the suitability on the use of digital AFC for the solution of this problem. Future research will be performed regarding the generation of the K_0 and g_k parameters by means of optimization methods taking into account the appropriate constraints and robustness indexes.

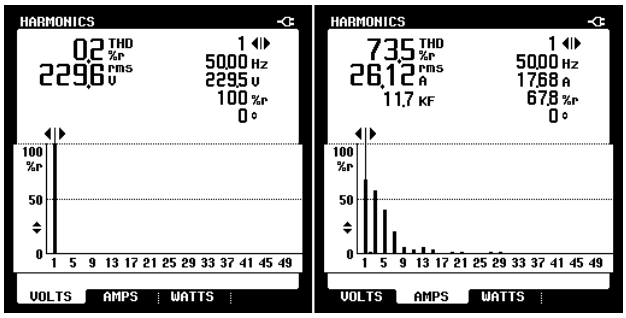

Fig. 10. THD measurement for the inverter feeding the nonlinear load (diode rectifier with R load and Co filter) at 4.0 kVA.

REFERENCES

M. Bodson. Rejection of periodic disturbances of unknown and time-varying frequency. *International Journal of Adaptive Control and Signal Processing*, 19(2-3):67–88, March 2005.

M. Bodson. Equivalence between adaptive cancellation algorithms and linear time-varying compensators. In *43rd IEEE Conference on Decision and Control, CDC*, volume 1, pages 638–643, 14-17 December 2004.

M. Bodson, A. Sacks, and P. Khosla. Harmonic generation in adaptive feedforward cancellation schemes. In *Proceedings of the 31st IEEE Conference on Decision and Control*, volume 2, pages 1261–1266, 16-18 December 1992.

M. Bodson, A. Sacks, and P. Khosla. Harmonic generation in adaptive feedforward cancellation schemes. *IEEE Transactions on Automatic Control*, 39(9):1939–1944, September 1994.

M.F. Byl, S.J. Ludwick, and D.L. Trumper. A loop shaping perspective for tuning controllers with adaptive feedforward cancellation. *Precision Engineering*, 29(1): 27–40, January 2005.

J. Doyle, B. Francis, and A. Tannenbaum. *Feedback Control Theory*, chapter 3: Basic Concepts, pages 27–38. Macmillan Publishing Co., 1990.

B. Francis and W. Mohan. Internal model principle in control theory. *Automatica*, 12:457–465, 1976.

D. G. Holmes and T. A. Lipo. *Pulse Width Modulation for Power Converters : Principles and Practice*, chapter 2: Harmonic Distortion, pages 57–93. Wiley-IEEE Press, 2003.

International Electrotechnical Commission IEC. IEC 62040-3 uninterruptible power systems (ups) - part 3: Method of specifying the performance and test requirements, annex e. International Electrotechnical Commission, Geneva, Switzerland, March 1999.

S.J. Ludwick. *A rotary fast tool servo for diamond turning of asymmetric optics*. PhD thesis, Department of Mechanical Engineering, Massachusetts Institute of Technology, Cambridge, MA., 1999.

W. Messner and M. Bodson. Design of adaptive feedforward controllers using internal model equivalence. In *American Control Conference*, volume 2, 1619-1623, 29 June-1 July 1994.

D.J. Pileggi, E.M. Gulachenski, C.E. Root, and A.E. Emanuel T.J. Gentile. The effect of modern compact fluorescent lights on voltage distortion. *IEEE Transactions on Power Delivery*, 8(3):1451–1459, July 1993.